1970

General circulation experiments with a two-level quasi-geostrophic model including the non-linear interaction between a single wave in the zonal direction and the mean flow

Taylor, Frank H.

Monterey, California ; Naval Postgraduate School

https://hdl.handle.net/10945/15016

GENERAL CIRCULATION EXPERIMENTS WITH A TWO-LEVEL QUASI-GEOSTROPHIC MODEL INCLUDING THE NON-LINEAR INTERACTION BETWEEN A SINGLE WAVE IN THE ZONAL DIRECTION AND THE MEAN FLOW

Frank H. Taylor

United States
Naval Postgraduate School

THESIS

GENERAL CIRCULATION EXPERIMENTS
WITH A TWO-LEVEL QUASI-GEOSTROPHIC MODEL
INCLUDING THE NON-LINEAR INTERACTION BETWEEN
A SINGLE WAVE IN THE ZONAL DIRECTION AND THE MEAN FLOW

by

Frank H. Taylor

April 1970

General Circulation Experiments With a Two-Level Quasi-Geostrophic Model Including the Non-Linear Interaction Between A Single Wave in the Zonal Direction and the Mean Flow

by

Frank H. Taylor
Lieutenant Commander, United States Navy
B.S.E.E., Purdue University, 1961

Submitted in partial fulfillment of the
requirements for the degree of

MASTER OF SCIENCE IN METEOROLOGY

from the

NAVAL POSTGRADUATE SCHOOL
April 1970

ABSTRACT

A long-period forecast is made utilizing a two-level quasi-geostrophic model. The model includes friction and heating which is a linear function of y. The model was further simplified by restricting the disturbance to one wave in the zonal direction. Experiments were performed with two distances between the walls. In the case of the longer separation, a solution with appreciable time fluctuations was obtained with the largest fluctuation being investigated in more detail. The smaller separation revealed a traveling wave of constant amplitude similar to that observed in certain dishpan experiments.

TABLE OF CONTENTS

I. INTRODUCTION 7

II. THE FORECAST EQUATIONS 10

III. BOUNDARY CONDITIONS AND FINITE DIFFERENCE SCHEME 15

IV. INITIAL CONDITIONS 17

V. RESULTS 18

VI. CONCLUSIONS 36

APPENDIX A - Computation of Vertical Motion 38

APPENDIX B - Computation of the Average North-South Wind 39

APPENDIX C - Energy Transformation Equations 40

LIST OF REFERENCES 43

INITIAL DISTRIBUTION LIST 45

FORM DD 1473 51

TABLE OF SYMBOLS AND ABBREVIATIONS

A_v	Vertical eddy viscosity
A_H	Horizontal eddy viscosity
β_o	Derivative of coriolis parameter at $y = 0$
C_p	Specific heat at constant pressure
f_o	Coriolis parameter at $y = 0$
g	Gravity
ω	dp/dt
Ψ	gz/f_o
R	Gas constant
ρ	Density
$\bar{T}$	Average temperature from standard atmosphere
σ	$(R^2\bar{T}/p^2g)\ (\partial\bar{T}/\partial z + g/C_p)$
ζ	$\nabla^2\Psi$
z	Height
$\varkappa$	R/C_p
Q	Heating added per unit mass
∇^4	Bi-harmonic operator $(\nabla^2)^2$
W	Distance between the walls

ACKNOWLEDGMENTS

The author wishes to express his deep gratitude to Dr. Roger Terry Williams whose recommendations, counsel, encouragement and infinite patience were great factors in the writing of this thesis.

I would further like to thank Dr. J. D. Mahlman for his suggestions and discussions which contributed to this study. A thank you is also offered to Commander R. L. Newman, USN and Captain T. K. Schminke, USAF, who cheerfully allowed portions of their basic models to be modified for the experiments conducted.

I. INTRODUCTION

Knowledge of the general circulation has been made possible with the advent of high-speed large-capacity electronic digital computers. In a classic experiment, Phillips [1956] performed a long-period numerical forecast with a two-level quasi-geostrophic model in a zonally periodic channel on a β plane. Friction and heating were included in his equations with the latter as a linear function of latitude. He introduced a finite amplitude initial disturbance into a baroclinically unstable zonal current. Major deficiencies were the error from the β plane and the geostrophic approximations, the latter making it impossible to account for non-geostrophic dynamics. Furthermore, due to computational errors, he did not achieve a statistically steady state. However, Phillips did initially demonstrate the feasibility of numerical simulation of the atmosphere.

General circulation experiments have progressed in sophistication and complexity since Phillips'. Smagorinsky [1963] formulated a two-level baroclinic primitive equation model by using the Eulerian equations of motion within a spherically zonal strip. Continued sophistication of the experiments resulted in a nine-level model utilizing the primitive equations of motion [Smagorinsky, Manabe and Holloway, 1965]. This study included a resolution of boundary layer fluxes and radiative transfer involving ozone, carbon dioxide and water vapor. A continuation of this study was performed for the tropics which was successful in simulating the tropical convergence zone and the thermal structure [Manabe and Smagorinsky, 1967]. Mintz

[1964] conducted an experiment in which the primitive equations of motion were developed for a two-level model of the atmosphere with the heating and friction terms retained. This model further brought in the effects of land-sea contrasts in heating. Nitta [1967] utilized a twenty-level model for computing vertical distribution of the geopotential flux and conversion of eddy potential energy and eddy kinetic energy due to non-stationary disturbances. A model which has the distinguishing feature of using height rather than pressure was developed [Kasahara and Washington, 1967] and hydrostatic equilibrium was maintained in the system. Some advantages of this model are the prognostic equations have a simpler form than those of the σ system and the lower boundary conditions may be easily formulated. The integration of the nine-level primitive equation model was further extended by the box method [Kurihara and Holloway, 1967] which conserved the conservational properties of the original equations. Recently, the effect of hydrology of the earth's surface was incorporated in the nine-level primitive equation model [Manabe, 1969]. The scheme involved the prediction of water vapor in the atmosphere and the prediction of soil moisture and snow cover. The numerical integrations were performed for the annual mean distribution of solar insolation.

The increased sophistication and complexity of recent models have also produced complex results which make interpretation difficult. Therefore, in this study, the complexities have been kept to a minimum while still maintaining a description of the basic dynamic processes. When the effects of heating and friction are included, the two-level quasi-geostrophic model is the simplest model capable of describing the general circulation.

The model is further simplified in that the disturbance is restricted to a single wave in the zonal direction. Phillips' [1956] experiments and Smagorinsky's [1963] experiment which contained no forcing function in the east-west direction, displayed a single predominate wave number which contained much of the disturbance energy. The y-structure of the disturbance and the mean flow are calculated accurately with a sufficient number of grid points. Some general circulation experiments have been made with even simpler models which represent the y-variation of all quantities with a few terms of a Fourier series [Bryan, 1959; Lorenz, 1962, 1963; Young, 1966]. These models do not provide an adequate description of the barotropic interaction between the disturbance and the mean flow. Consequently, this model appears to be the simplest model which can describe the main mechanisms of the general circulation of the atmosphere.

II. THE FORECAST EQUATIONS

A simple two-level model is constructed by dividing the entire atmosphere into four layers of constant pressure differential, $\frac{\Delta p}{2}$ (fig. 1), numbered 0 to 4 from top to bottom. Assume vertical motion to be zero at the top of the atmosphere, while

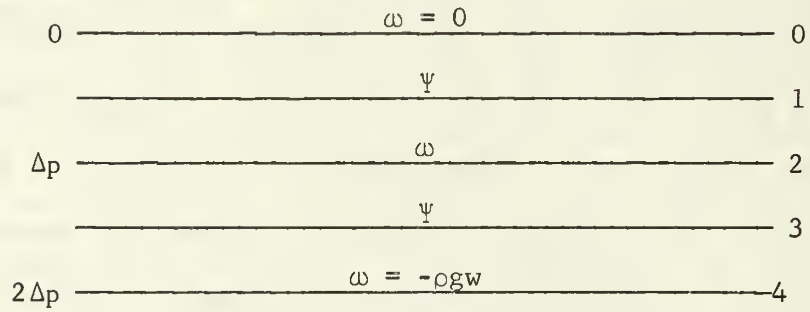

Fig. 1. Two-level model used for prediction .

the vertical motion term at the earth's surface is approximated by

$$\omega \cong -\rho g w_4 . \tag{2.1}$$

Charney and Eliassen [1949] used the Ekman theory to derive an expression for w_4 which is

$$w_4 = \frac{1}{2}\left(\frac{2\,A_v}{f_o}\right)^{1/2} \sin 2\,\alpha\,\zeta_4 , \tag{2.2}$$

where A_v is the vertical eddy viscosity and α, the inflow angle. The surface geostrophic vorticity is approximated by

$$\zeta_4 \cong \zeta_3 = \nabla^2\,\Psi_3 . \tag{2.3}$$

Following the development of Thompson [1961], but with different notation, begin with the quasi-geostrophic vorticity equation

$$\frac{\partial}{\partial t}\,\nabla^2\Psi + \mathbb{k} \times \nabla\Psi\cdot\nabla(\nabla^2\Psi) + \beta_o\,\frac{\partial\Psi}{\partial x} - f_o\,\frac{\partial\omega}{\partial p} = A_H\,\nabla^4\Psi . \tag{2.4}$$

Apply this equation at levels 1 and 3 giving

$$\frac{\partial}{\partial t} \nabla^2 \Psi_1 + \mathbb{k} \times \nabla\Psi_1 \cdot \nabla(\nabla^2\Psi_1) + \beta_o \frac{\partial \Psi_1}{\partial x} - f_o \frac{\omega_2}{\Delta p} = A_H \nabla^4 \Psi_1, \qquad (2.5)$$

$$\frac{\partial}{\partial t} \nabla^2 \Psi_3 + \mathbb{k} \times \nabla\Psi_3 \cdot \nabla(\nabla^2\Psi_3) + \beta_o \frac{\partial \Psi_3}{\partial x} + f_o \frac{(\omega_4 - \omega_2)}{\Delta p} = A_H \nabla^4 \Psi_3. \qquad (2.6)$$

If it is desired to stop at some intermediate point, say the tropopause, smaller layers could be utilized rather than to include the entire atmosphere.

Next consider the quasi-geostrophic first law of thermodynamics in the form

$$\frac{\partial}{\partial t} \frac{\partial \Psi}{\partial p} + \mathbb{k} \times \nabla\Psi \cdot \nabla \left(\frac{\partial \Psi}{\partial p}\right) + \frac{\sigma}{f_o} \omega = - \frac{\varkappa}{f_o p} Q. \qquad (2.7)$$

where

$$\sigma = \frac{R^2 T_s}{p^2 g} \left[\frac{\partial T_s}{\partial z} + \frac{g}{C_p}\right]. \qquad (2.7a)$$

and T_s is the temperature from the standard atmosphere. When this equation is applied at level 2, the result is

$$\frac{\partial}{\partial t} (\Psi_1 + \Psi_3) + \mathbb{k} \times \nabla \frac{(\Psi_1 + \Psi_3)}{2} \cdot \nabla(\Psi_1 - \Psi_3) - \frac{\Delta p \ \sigma \omega_2}{f_o} = \frac{\varkappa}{f_o} Q_2. \qquad (2.8)$$

Define the following quantities

$$\Psi_m = \frac{\Psi_1 + \Psi_3}{2}, \qquad (2.9)$$

$$\Psi_T = \frac{\Psi_1 - \Psi_3}{2}, \qquad (2.10)$$

which implies

$$\Psi_1 = \Psi_m + \Psi_T, \qquad (2.11)$$

$$\Psi_3 = \Psi_m - \Psi_T. \qquad (2.12)$$

Here Ψ_T is proportional to the layer thickness and is therefore a measure of the mean temperature. Using these definitions, add (2.5) and (2.6) and divide the result by 2, obtaining

$$\frac{\partial}{\partial t} \nabla^2 \Psi_m + \mathbb{k} \times \nabla\Psi_m \cdot \nabla(\nabla^2 \Psi_m) + k \times \Psi_T \cdot \nabla(\nabla^2 \Psi_T) + \beta_o \frac{\partial \Psi_m}{\partial x} - f_o \frac{\omega_4}{2\Delta p}$$

$$= A_H \nabla^4 \Psi_m . \tag{2.13}$$

For the second forecast equation, subtract (2.6) from (2.5) and eliminate ω_2 using (2.8)

$$\frac{\partial}{\partial t} (\nabla^2 - \mu^2) \Psi_T + \mathbb{k} \times \nabla\Psi_m \cdot \nabla(\nabla^2 - \mu^2) \Psi_T + k \times \nabla\Psi_T \cdot \nabla(\nabla^2 \Psi_m)$$

$$+ \beta_o \frac{\partial \Psi_T}{\partial x} + f_o \frac{\omega_4}{2\Delta p} = - \mu^2 \frac{\varkappa Q_2}{2 f_o} + A_H \nabla^4 \Psi_T , \tag{2.14}$$

where

$$\mu^2 = \frac{2 f_o^2}{\Delta p^2 \sigma} . \tag{2.14a}$$

These are the prediction equations for the model. At this point we restrict ourselves to a disturbance of wave number k and the mean flow. The fields may be defined as follows

$$\Psi_m = E(y,t) + A(y,t) \cos kx + B(y,t) \sin kx, \tag{2.15}$$

$$\Psi_T = F(y,t) + C(y,t) \cos kx + D(y,t) \sin kx, \tag{2.16}$$

where k is the x wave number, A through D are Fourier amplitudes of the disturbance and E and F are the zonal mean fields. Now substitute expressions for Ψ_m and Ψ_T into (2.13), separate the various terms, neglecting all terms with wave number 2k or higher. Equating coefficients of the cosine terms gives

$$\frac{\partial}{\partial t}\left(\frac{\partial^2 A}{\partial y^2} - Ak^2\right) = k \left[\frac{\partial E}{\partial y} \frac{\partial^2 B}{\partial y^2} + \frac{\partial F}{\partial y} \frac{\partial^2 D}{\partial y^2} - \frac{\partial^3 E}{\partial y^3} B - \frac{\partial^3 F}{\partial y^3} D - \right.$$

$$\left. k^2 \left(\frac{\partial E}{\partial y} B + \frac{\partial F}{\partial y} D\right)\right] - \beta_o Bk - K\left(\frac{\partial^2}{\partial y^2} - k^2\right) (A-C) +$$

$$A_H \left[\frac{\partial^4 A}{\partial y^4} - 2k^2 \frac{\partial^2 A}{\partial y^2} + k^4 A\right]. \tag{2.17}$$

For the sine terms the result is

$$\frac{\partial}{\partial t}\left(\frac{\partial^2 B}{\partial y^2} - Bk^2\right) = k\left[-\frac{\partial E}{\partial y}\frac{\partial^2 A}{\partial y^2} - \frac{\partial F}{\partial y}\frac{\partial^2 C}{\partial y^2} + \frac{\partial^3 E}{\partial y^3} A + \frac{\partial^3 F}{\partial y^3} C + k^2\left(\frac{\partial E}{\partial y} A + \frac{\partial F}{\partial y} C\right)\right] + \beta_o Ak - K\left(\frac{\partial^2}{\partial y^2} - k^2\right)(B-D) + A_H\left[\frac{\partial^4 B}{\partial y^4} - 2k^2\frac{\partial^2 B}{\partial y^2} - k^4 B\right]. \quad (2.18)$$

Repeating the procedures for (2.14), the equations are

$$\frac{\partial}{\partial t}\left(\frac{\partial^2 C}{\partial y^2} - Ck^2 - C\mu^2\right) = k\left[\frac{\partial E}{\partial y}\frac{\partial^2 D}{\partial y^2} + \frac{\partial F}{\partial y}\frac{\partial^2 B}{\partial y^2} - \frac{\partial E}{\partial y} D\,(k^2+\mu^2) - \frac{\partial F}{\partial y} B\,(k^2-\mu^2) - \frac{\partial^3 E}{\partial y^3} D - \frac{\partial^3 F}{\partial y^3} B\right] - \beta_o Dk + K\left(\frac{\partial^2}{\partial y^2} - k^2\right)(A-C) + A_H\left[\frac{\partial^4 C}{\partial y^4} - 2k^2\frac{\partial^2 C}{\partial y^2} + k^4 C\right], \quad (2.19)$$

and

$$\frac{\partial}{\partial t}\left(\frac{\partial^2 D}{\partial y^2} - Dk^2 - D\mu^2\right) = k\left[\frac{\partial E}{\partial y} C\,(k^2+\mu^2) + \frac{\partial F}{\partial y} A\,(k^2-\mu^2) - \frac{\partial E}{\partial y}\frac{\partial^2 C}{\partial y^2} - \frac{\partial F}{\partial y}\frac{\partial^2 A}{\partial y^2} + \frac{\partial^3 F}{\partial y^3} A + \frac{\partial^3 E}{\partial y^3} C\right] + \beta_o Ck + K\left(\frac{\partial^2}{\partial y^2} - k^2\right)(B-D) + A_H\left[\frac{\partial^4 D}{\partial y^4} - 2k^2\frac{\partial^2 D}{\partial y^2} + k^4 D\right]. \quad (2.20)$$

Equating coefficients of terms independent of x in (2.13) gives

$$\frac{\partial}{\partial t}\frac{\partial^2 E}{\partial y^2} = \frac{k}{2}\frac{\partial}{\partial y}\left[A\frac{\partial^2 B}{\partial y^2} - B\frac{\partial^2 A}{\partial y^2} + C\frac{\partial^2 D}{\partial y^2} - D\frac{\partial^2 C}{\partial y^2}\right] -$$

$$K\frac{\partial}{\partial y}\left(\frac{\partial E}{\partial y} - \frac{\partial F}{\partial y}\right) + A_H\frac{\partial}{\partial y}\left(\frac{\partial^3 E}{\partial y^3}\right). \tag{2.21}$$

Similarly, coefficients indepdendent of x in (2.14) results in

$$\left(\frac{\partial^2}{\partial y^2} - \mu^2\right)\frac{\partial F}{\partial y} = \frac{k}{2}\frac{\partial}{\partial y}\left[A\frac{\partial^2 D}{\partial y^2} - B\frac{\partial^2 C}{\partial y^2} + C\frac{\partial^2 B}{\partial y^2} - D\frac{\partial^2 A}{\partial y^2} +\right.$$

$$\left.\mu^2\left(B\frac{\partial C}{\partial y} + C\frac{\partial B}{\partial y} - A\frac{\partial D}{\partial y} - D\frac{\partial A}{\partial y}\right]\right. +$$

$$K\left(\frac{\partial E}{\partial y} - \frac{\partial F}{\partial y}\right) - \frac{\mu^2 \varkappa Q_2}{2} + A_H\frac{\partial}{\partial y}\left(\frac{\partial^3 F}{\partial y^3}\right), \tag{2.22}$$

where

$$K = \frac{f_o g}{2R\bar{T}}\left(\frac{A_m}{f_o}\right)^{1/2} . \tag{2.23}$$

The prediction equations are now in the form to be used in the model.

III. FINITE DIFFERENCE SCHEME AND BOUNDARY CONDITIONS

The finite difference scheme used is illustrated below with a sample variable N;

$$\frac{\partial N}{\partial y} = \frac{1}{2H}\left(N_{i+1} - N_{i-1}\right) \tag{3.1}$$

$$\frac{\partial^2 N}{\partial y^2} = \frac{1}{H^2}\left(N_{i+1} - 2N_i + N_{i-1}\right) \tag{3.2}$$

$$\frac{\partial^3 N}{\partial y^3} = \frac{1}{2H^3}\left[\left(N_{i+2} - 2N_{i+1} + N_i\right) - \left(N_i - 2N_{i-1} + N_{i-2}\right)\right] \tag{3.3}$$

where i is the grid index and H the distance between grid points.

Centered time differences are used for all quantities except those involving friction. The frictional terms are computed at time ($t-\Delta t$). In all cases the first step was a forward time step. A special time step was introduced every 24 time steps to avoid the separation of solutions at even and odd time steps. These special time steps used the backwards difference method utilized by Matsuno [1966]. Second order equations (2.17), (2.18), (2.19) and (2.20) for time tendencies are solved by the exact method of Richtmyer [1957]. A modification of the Richtmyer method used by Phillips [1956] was necessary for equation (2.22) to satisfy the boundary conditions. Equation (2.21) was solved by a direct marching process utilizing the boundary conditions.

The following boundary conditions were established:

The quantities A through D = 0

$\frac{\partial}{\partial t}\frac{\partial F}{\partial y} = 0$ and $\frac{\partial}{\partial t}\frac{\partial E}{\partial y} = 0$ all at $y = 0$ and $y = W$.

Following Phillips [1956] the mean and disturbance vorticity are set equal to zero at the boundary in order to make the boundary walls smooth.

IV. INITIAL CONDITIONS

A natural initial state would be one of constant temperature and no motion. The heating, in time, would build up a baroclinic current. No disturbance could develop until the vertical shear of the zonal current reached a critical value. In order to save computer time, the initial state was chosen to consist of a zonal current with a vertical shear near the critical value [see Thompson, 1961]. The initial disturbance has a wave length and a y-structure such that when superimposed on a baroclinic current with no horizontal shear it would have maximum growth rate.

The initial conditions for the model are

$$A = 200 \sin \frac{\pi y}{W}$$

$$B \text{ through } D = 0$$

$$F = \frac{f_o HW6}{\pi} \cos \frac{\pi y}{W}$$

$$E = \frac{f_o HW6}{\pi} \cos \frac{\pi y}{W} .$$

V. RESULTS

The main experiments were conducted using the physical parameters listed in Table I.

f_o	$= 1 \times 10^{-4}$ per second
σ	= 2.3 meters squared per second squared per centibar squared
β	$= 1.67 \times 10^{-11}$ per meter per second
Δp	= 50 centibars
A_v	= 40 meters squared per second
A_H	$= 1 \times 10^{5}$ meters squared per second
α	= 22.5 degrees
μ^2	$= 2.49 \times 10^{-12}$ per meter squared
H	= 200 kilometers
Δt	= 0.5 hours
k	$= 2\pi/4000$ per kilometer

Table I - Numerical Values of the Physical Constants

The variation of experiments 2 and 3 from the main experiment is tabulated in Table II.

	W (Km)	Q (Kj per ton per sec)
Experiment 1	8000	$4 \times 10^{-3} \left(y - \frac{W}{2}\right)/W$
Experiment 2	8000	$8 \times 10^{-3} \left(y - \frac{W}{2}\right)/W$
Experiment 3	4000	$8 \times 10^{-3} \left(y - \frac{W}{2}\right)/W$

Table II - Variation of the Physical Parameters

The forecast period for all three experiments was 300 days. Figure 2 depicts a plot of the disturbance energy for the 300 day forecast period. The disturbance energy referred to throughout the discussion is defined in Appendix C (Eqs. C-10 and C-11). A main feature of Fig. 2 is that the disturbance energy does not reach a steady state although it appears to be statistically stable after the first 120 days.

Figure 3 displays a time section of the mean wind for the period 120-260 days which is the main time period of interest for this experiment. The general increase of the disturbance energy begins to level off near day 140 which corresponds to the initial appearance of the southern jet. This result is similar to observations of Riehl, Yeh and LaSeur [1950]. The period between day 190 and day 200 is of considerable interest. The disturbance energy has its greatest fluctuations during this period and it corresponds to the termination of the southern jet.

Figures 4 - 7 represent the amplitudes and phases of Ψ_m, Ψ_T and w_2 in the form $P\cos(kx-\delta)$ where P is the amplitude and δ is the phase. Figures 4 and 5 represent day 190, prior to the disturbance peak, and Figs. 6 and 7 correspond to day 196, after the peak. The necessary condition for barotropic instability is that $\beta - \frac{\partial^2 \Psi_1}{\partial y^2}$ change sign somewhere in the region [Kuo, 1949]. Calculation at day 190 showed that this condition was satisfied in the vicinity of the southern jet. It is seen in the lower portion of Fig. 4, between y = 1000 km and y = 2500 km, that the phase tilts of Ψ_m, Ψ_T and w_2 are opposite to the shear of $\bar{u}_1$. These phase relationships indicate barotropic amplification and therefore a transformation of energy from the mean flow to the disturbance. However, the northern portion of Fig. 4 shows the

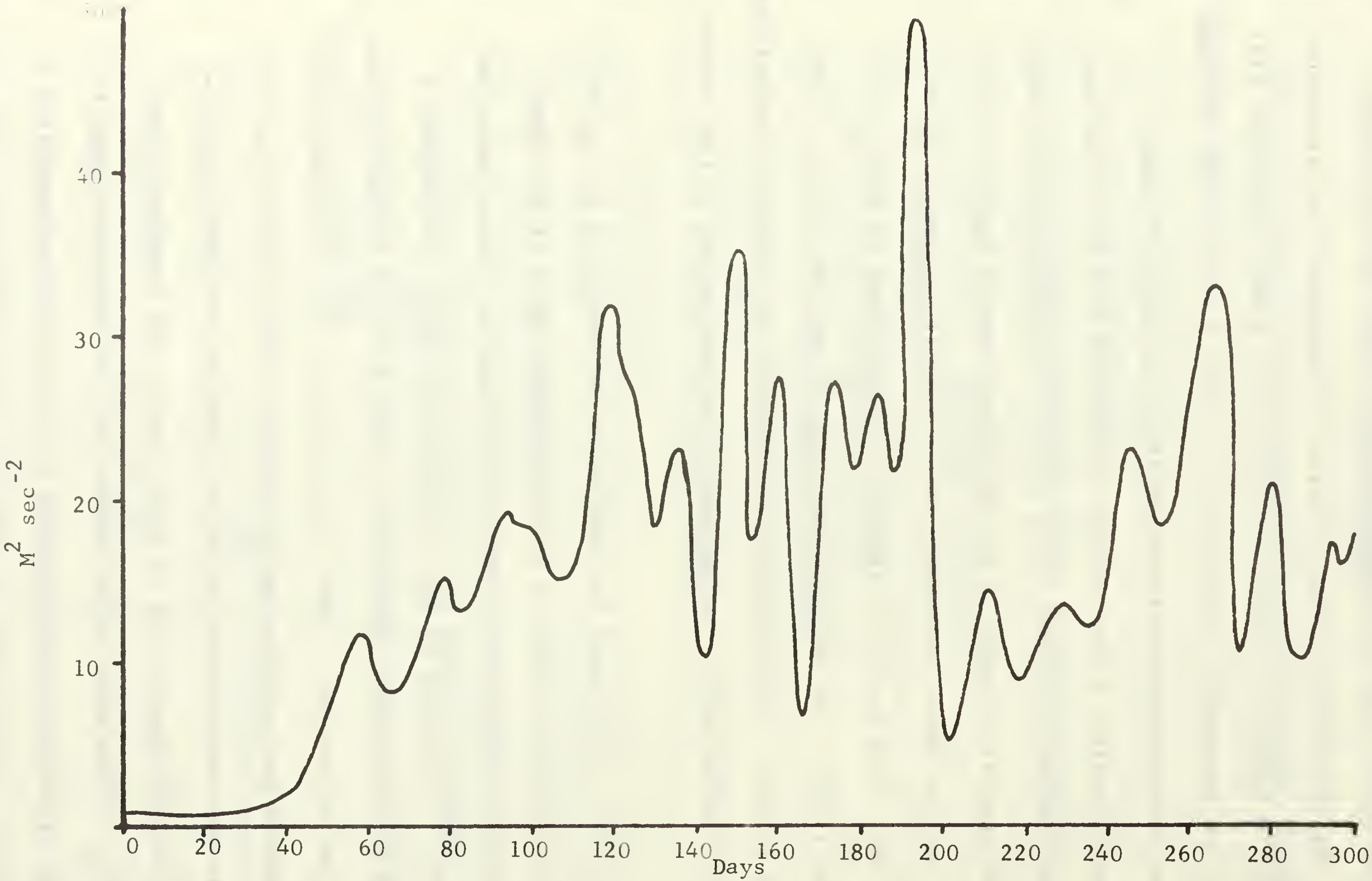

Fig. 2 - The Disturbance Energy of Experiment 1 for the Forecast Period.

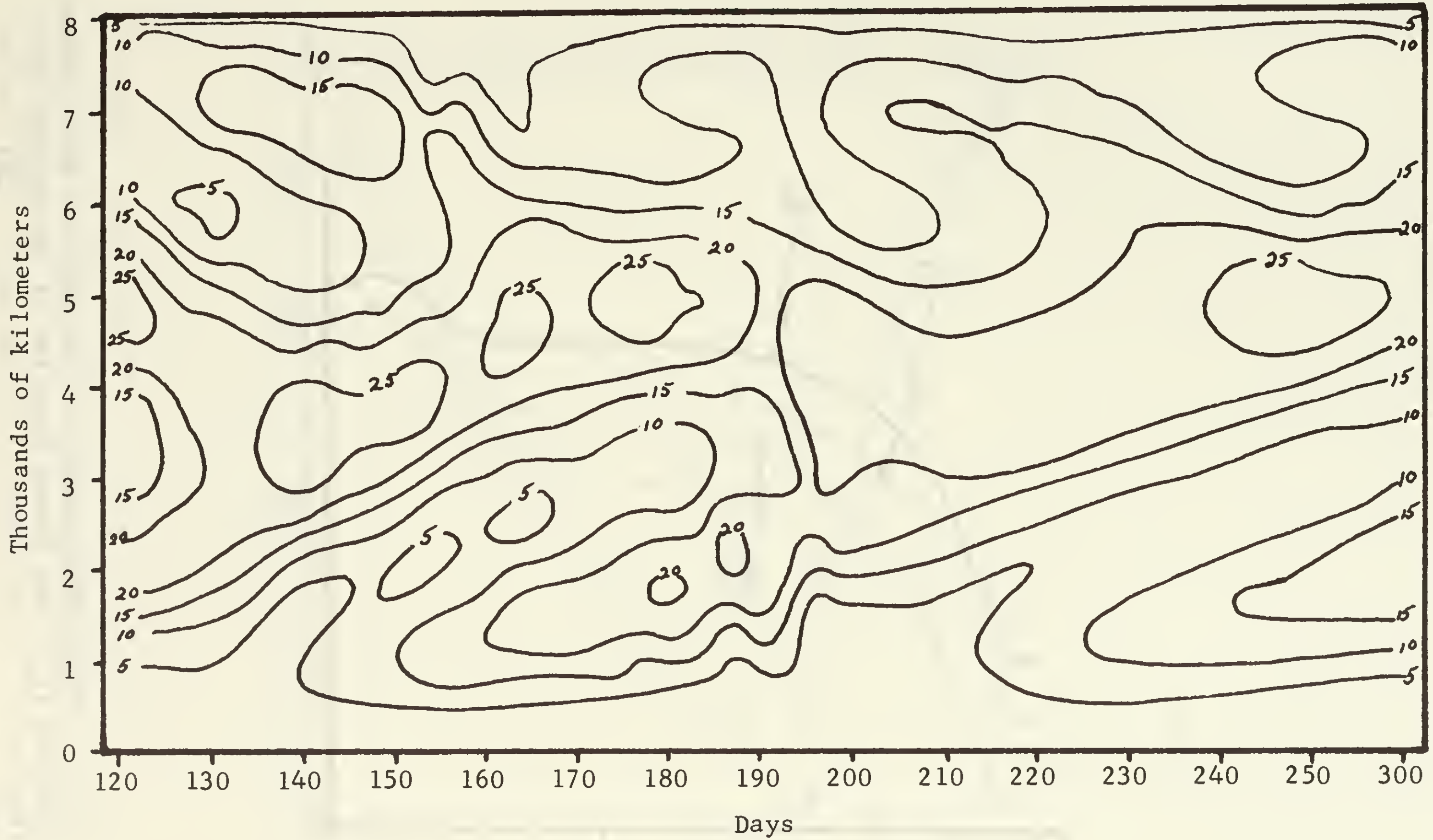

Fig. 3 - Time Cross Section of the Mean Zonal Wind at Level 1.

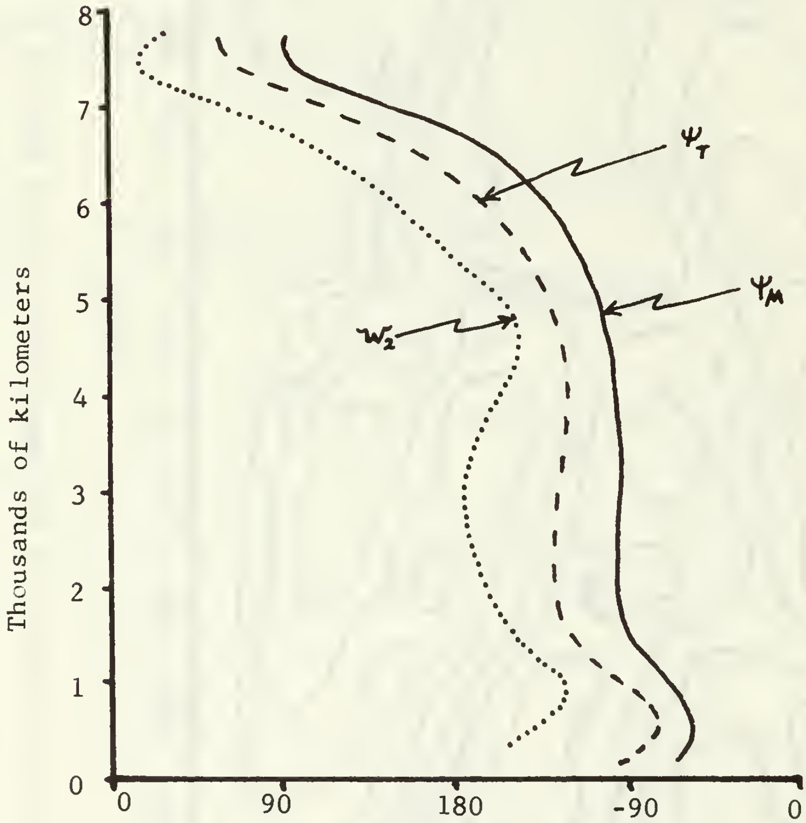

Fig. 4 - Phase Relationship of the Vertical Mean Stream Function (Ψ_m), the Stream Function of the Thermal Wind (Ψ_T) and the Vertical Motion ($w_2 = -\frac{\omega 2}{\rho g}$) for day 190.

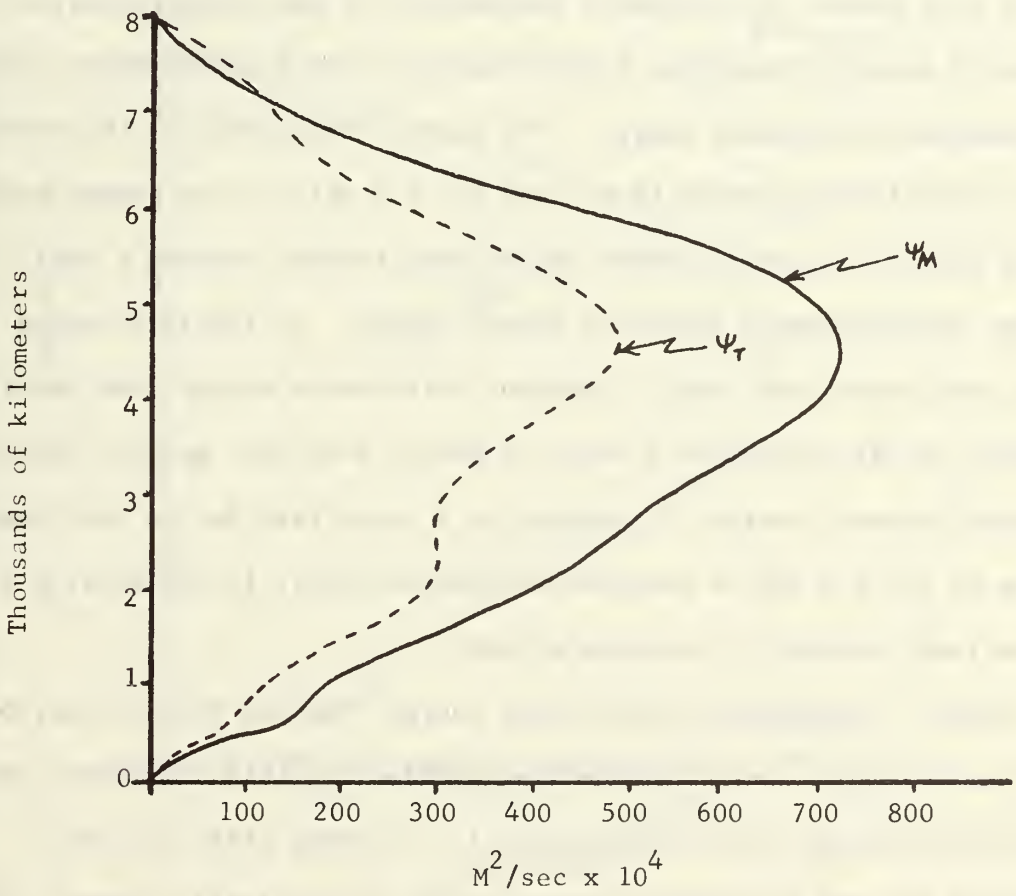

Fig. 5 - Amplitude of Ψ_m and Ψ_T for day 190.

same tilt as the shear of $\bar{u}_1$ which indicates barotropic damping: this implies an energy transformation of disturbance kinetic energy to mean kinetic energy. Figure 5 portrays the amplitude of Ψ_m and Ψ_T; clearly Ψ_m is larger and both fields have a mid-latitude maximum. A secondary peak of amplitude in Ψ_T is beginning to form which is a product of the barotropic instability. Figure 6 shows that all parameters (Ψ_m, Ψ_T, w_2) have a phase tilt which indicates barotropic damping over the entire range. The amplitude of Ψ_m and Ψ_T corresponding to Fig. 6 are displayed in Fig. 7. Of primary note is the distinct double maximum of amplitude which is a result of barotropic instability in the southern region. Figure 8 depicts the energy transformations over a period which includes the maximum disturbance energy. The first item of note is the nearly exact correlation between $[\bar{P} \cdot P']$ and $[P' \cdot K']$ which in an energy balance would almost completely offset one another thereby leaving a small amount of disturbance potential energy change. It should be noted that just before the event of maximum disturbance energy, the barotropic damping $[K' \cdot \bar{K}]$ approached a value of zero. This fact permits the disturbance kinetic energy to increase at a rapid rate due to the large value of $[P' \cdot K']$ and to continue to increase until $[K' \cdot \bar{K}]$ attains a value large enough to terminate growth.

Figure 9 depicts the disturbance energy over the forecast period for experiment 2. As stated earlier (Table II), this experiment has twice the heating rate of experiment 1. A steady state was not attained but the disturbance energy became statistically steady. The main differences from experiment 1 are that the disturbance energy fluctuates more rapidly and that its magnitude is much higher.

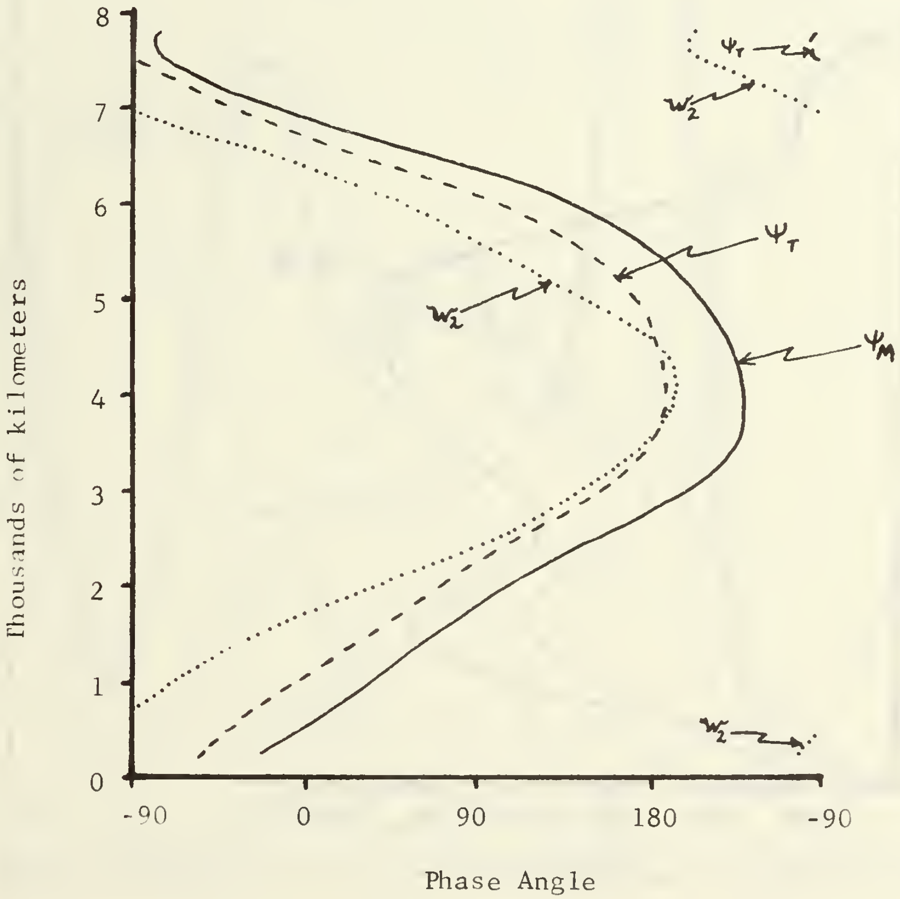

Fig. 6 - Phase Relationship of Ψ_m, Ψ_T and w_2 for day 196.

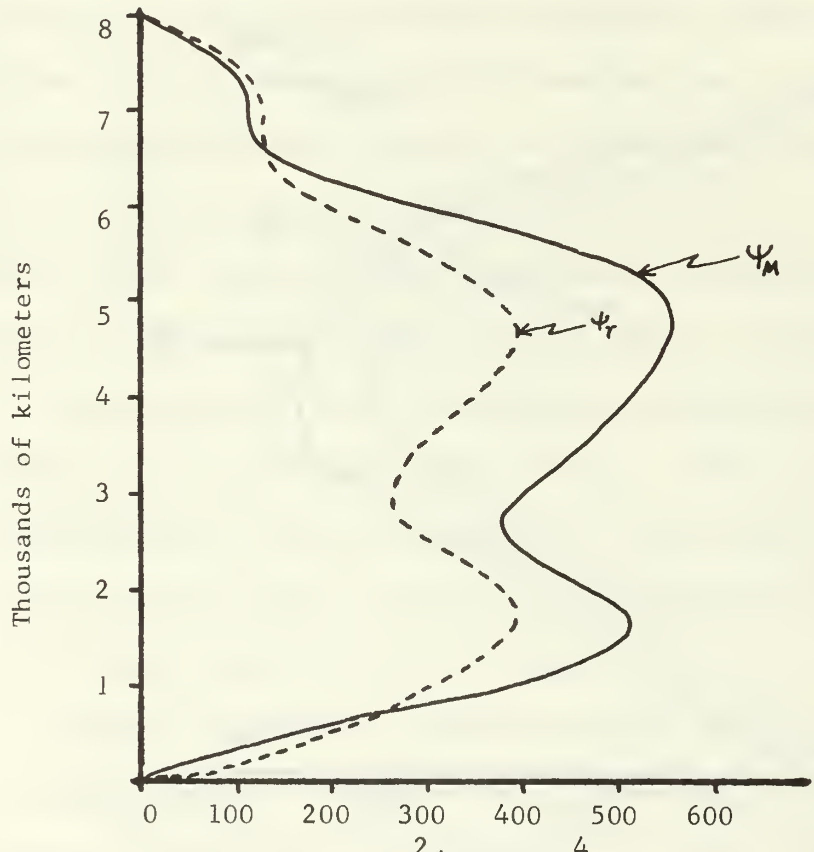

Fig. 7 - Amplitude of Ψ_m and Ψ_T for day 196.

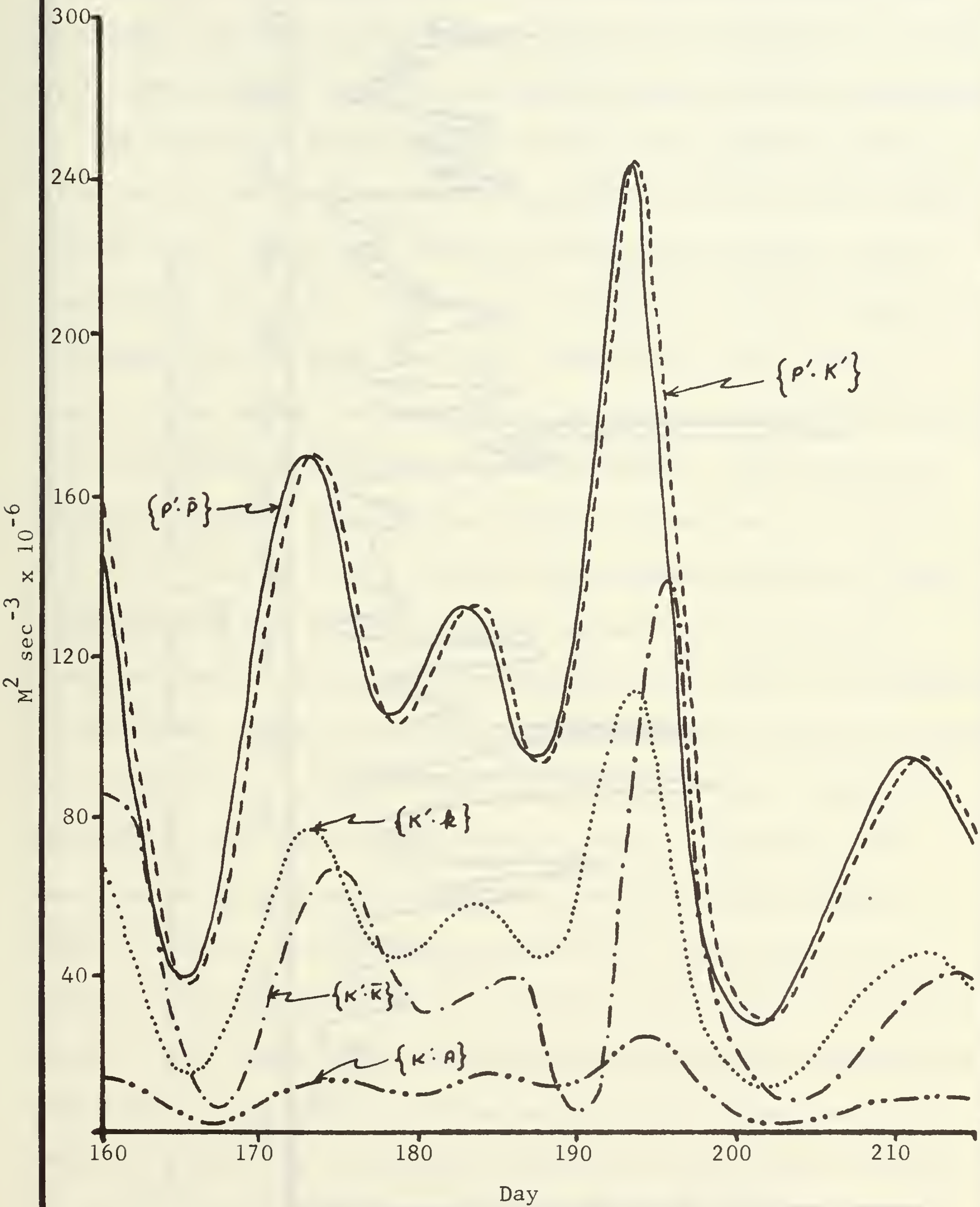

Fig. 8 - Energy Transformation for Period which Includes the Event of Maximum Disturbance.

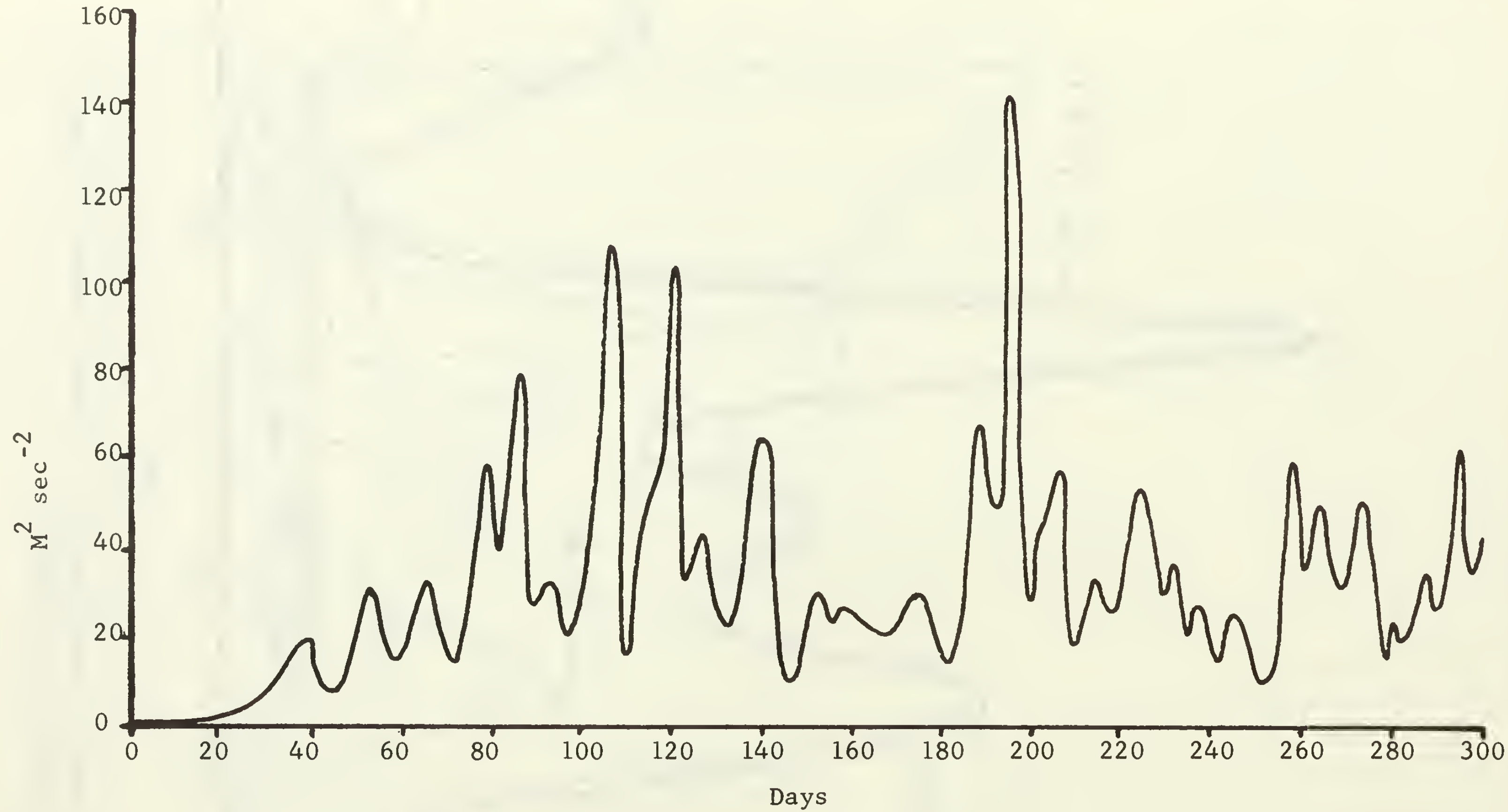

Fig. 9 - The Disturbance Energy of Experiment 2 for the Forecast Period.

A depiction of the disturbance energy over the forecast period for experiment 3 is contained in Fig. 10. This experiment differs from experiment 1 in that the disturbance between the walls has been cut in half. The heating coefficient was doubled from its value in experiment 1. The disturbance energy reached a steady state condition shortly after day 120 and stayed relatively constant to the end of the period. Thus we have a single wave traveling through the atmosphere with no variation in amplitude. This result is similar to certain dishpan experiments with an inner core [Hide, 1953; Fultz, et al, 1959]. Figure 11 represents the phases of Ψ_m, Ψ_T and w_2 at day 200 and reveals that the parameters have similar phase variations. The phase tilts indicate barotropic damping since there is a single jet in $\bar{u}_1$ (see Fig. 13). Since Ψ_T lags Ψ_m, there is a northward heat flux and energy transformation from the mean potential energy to the disturbance potential energy. The correlation mentioned above gives a transformation of disturbance potential energy to disturbance kinetic energy since there is a tendency for cold air to sink and warm air to rise. Figure 12 represents a plot of the amplitudes of Ψ_m and Ψ_T at day 200. The amplitude of Ψ_m is greater than Ψ_T and both have a single maximum. Figure 13 depicts the relationship between $\bar{u}_3$, which could be considered the surface wind, and $\bar{u}_1$ at day 200. This mean wind field is similar to that observed in the atmosphere, although the gradients are much less. At the surface, $\bar{u}$ is westerly in the mid latitudes and easterly at high and low latitudes while at the upper levels the flow is westerly with a mid-latitude jet. Figure 14 is a plot of the amplitude of the mean meridional component of the wind ($\bar{v}_1$) for day 200. The amplitude of $\bar{v}_1$ reveals a northerly component at mid latitudes and a southerly component at high and low latitudes which implies an indirect Ferrel circulation at mid latitudes and a direct Hadley circulation at high and low latitudes.

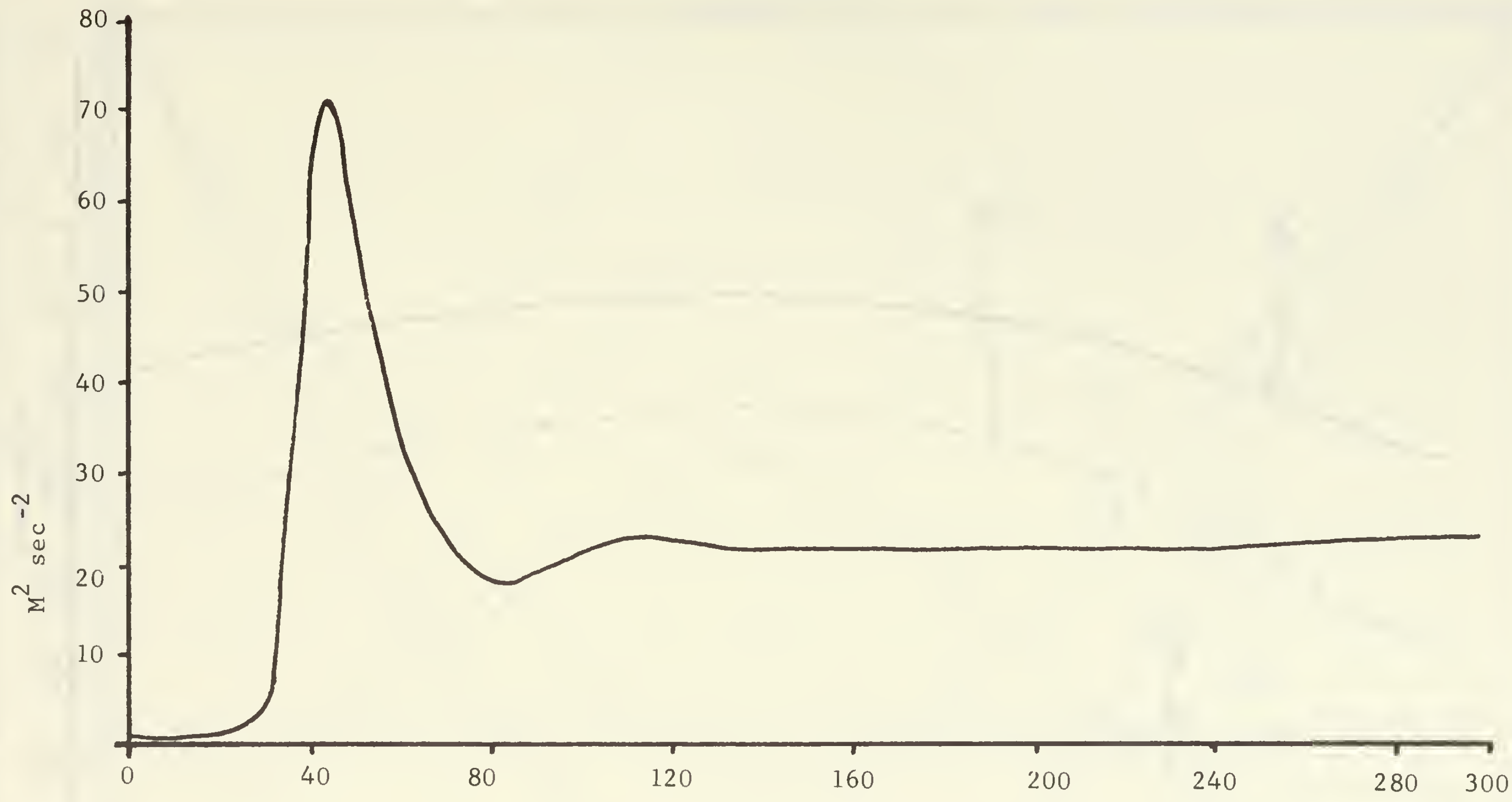

Fig. 10 - The Disturbance Energy for Experiment 3 for the Forecast Period.

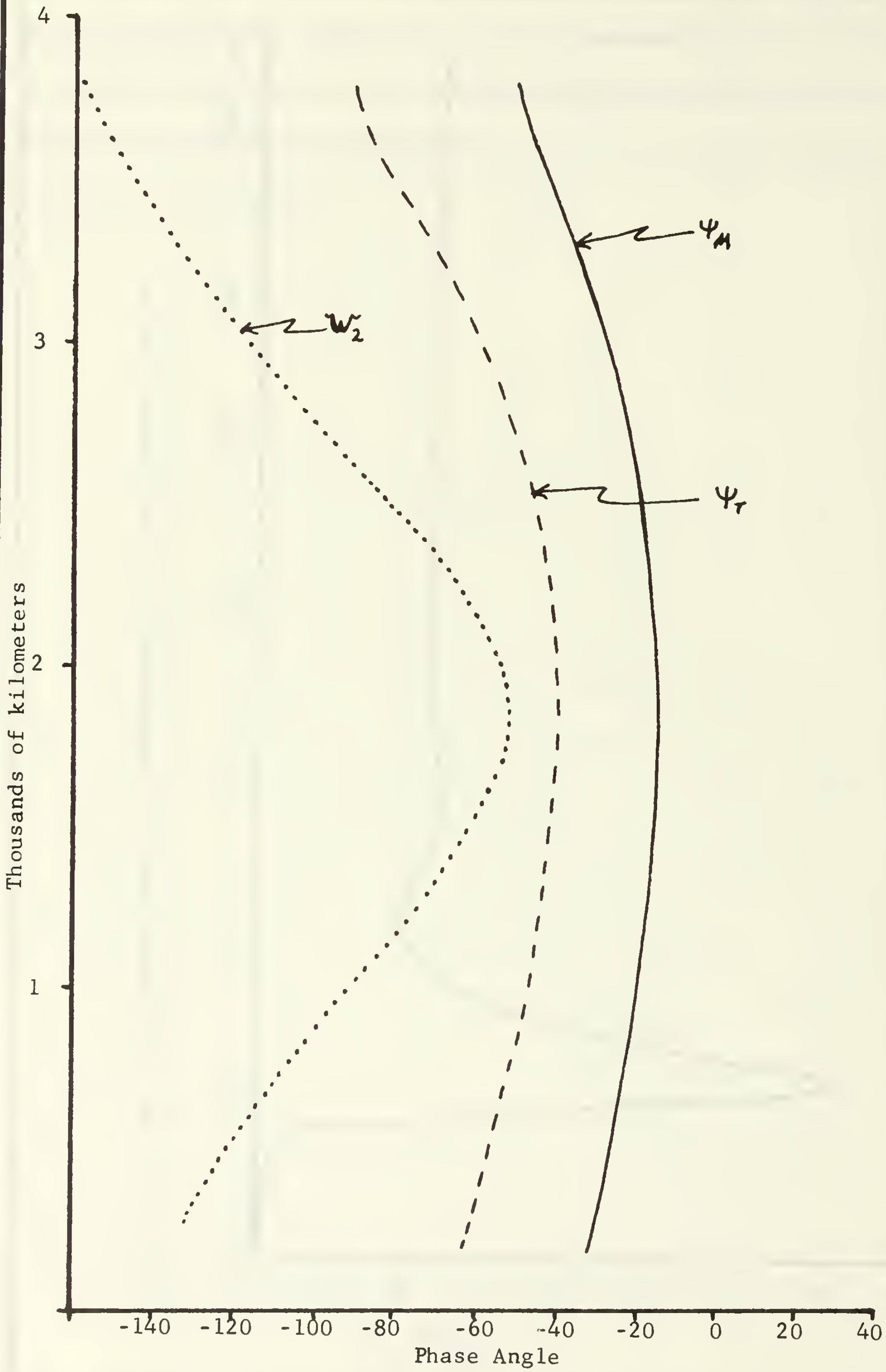

Fig. 11 - The Phase Relationship of Ψ_m, Ψ_T and w_2 for day 200.

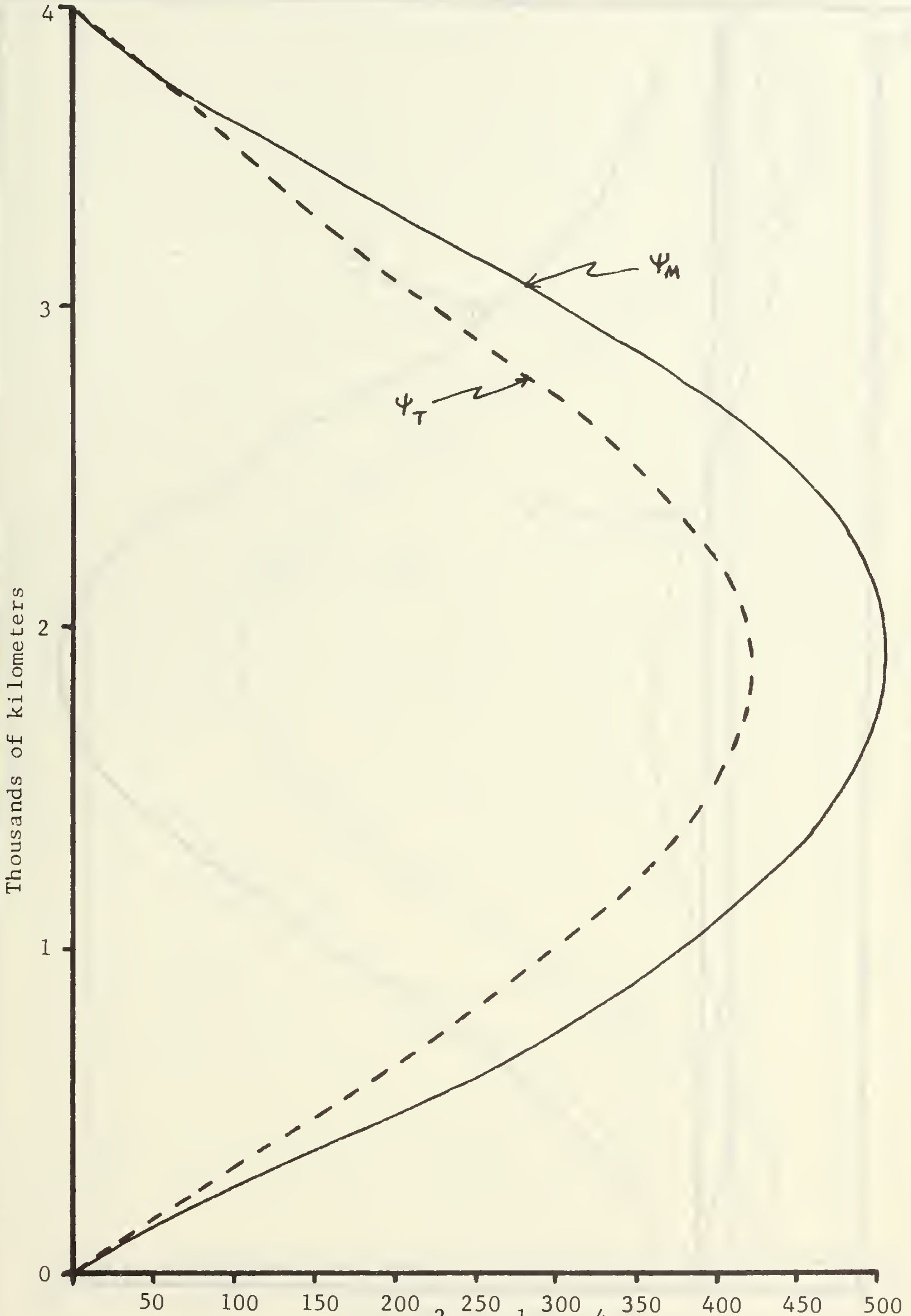

Fig. 12 - The Amplitude of Ψ_m and Ψ_T for day 200.

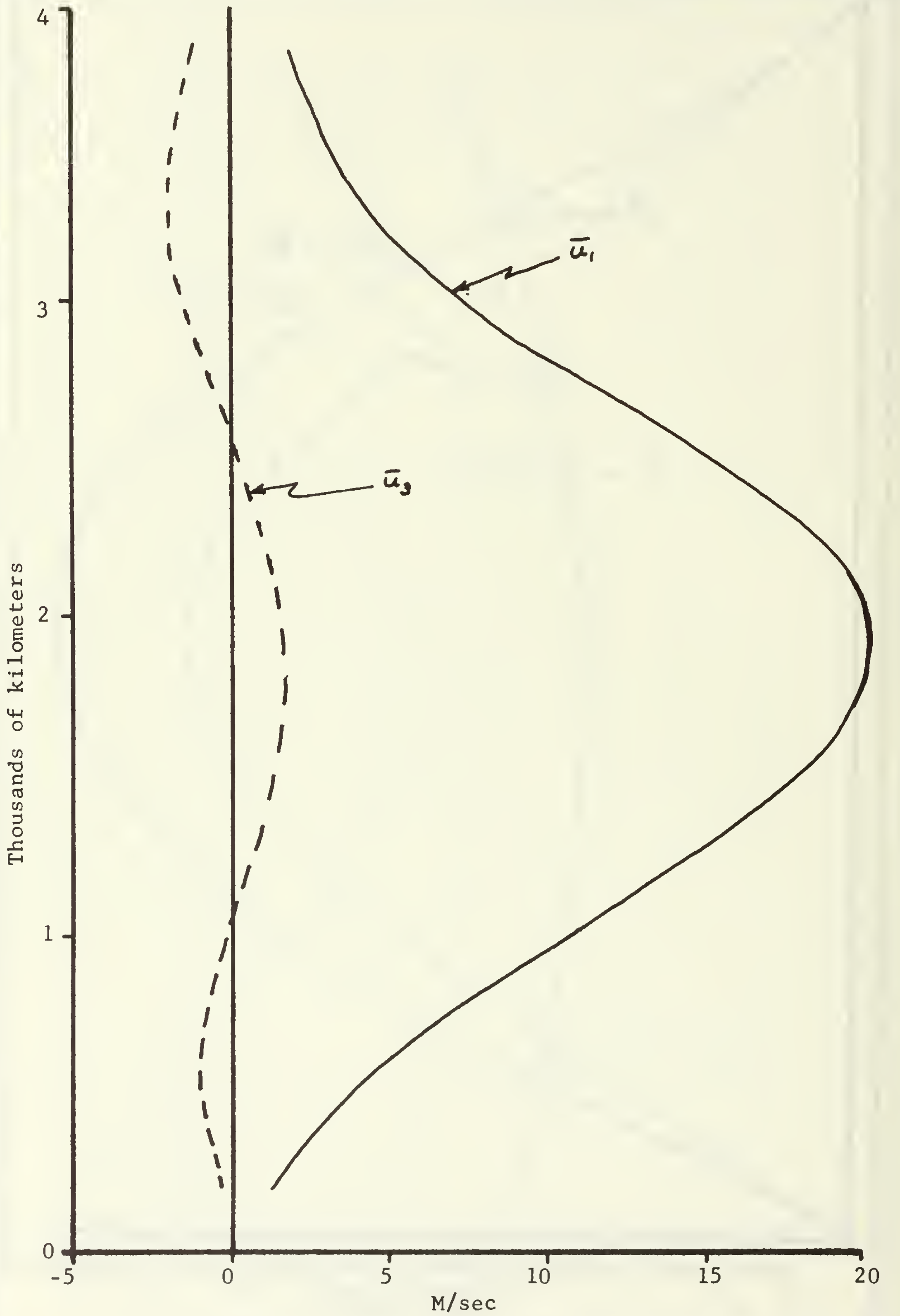

Fig. 13 - The Amplitude of the Zonal Component of the mean $(\bar{u}_1)$ and the Mean Surface Wind $(\bar{u}_3)$ for day 200.

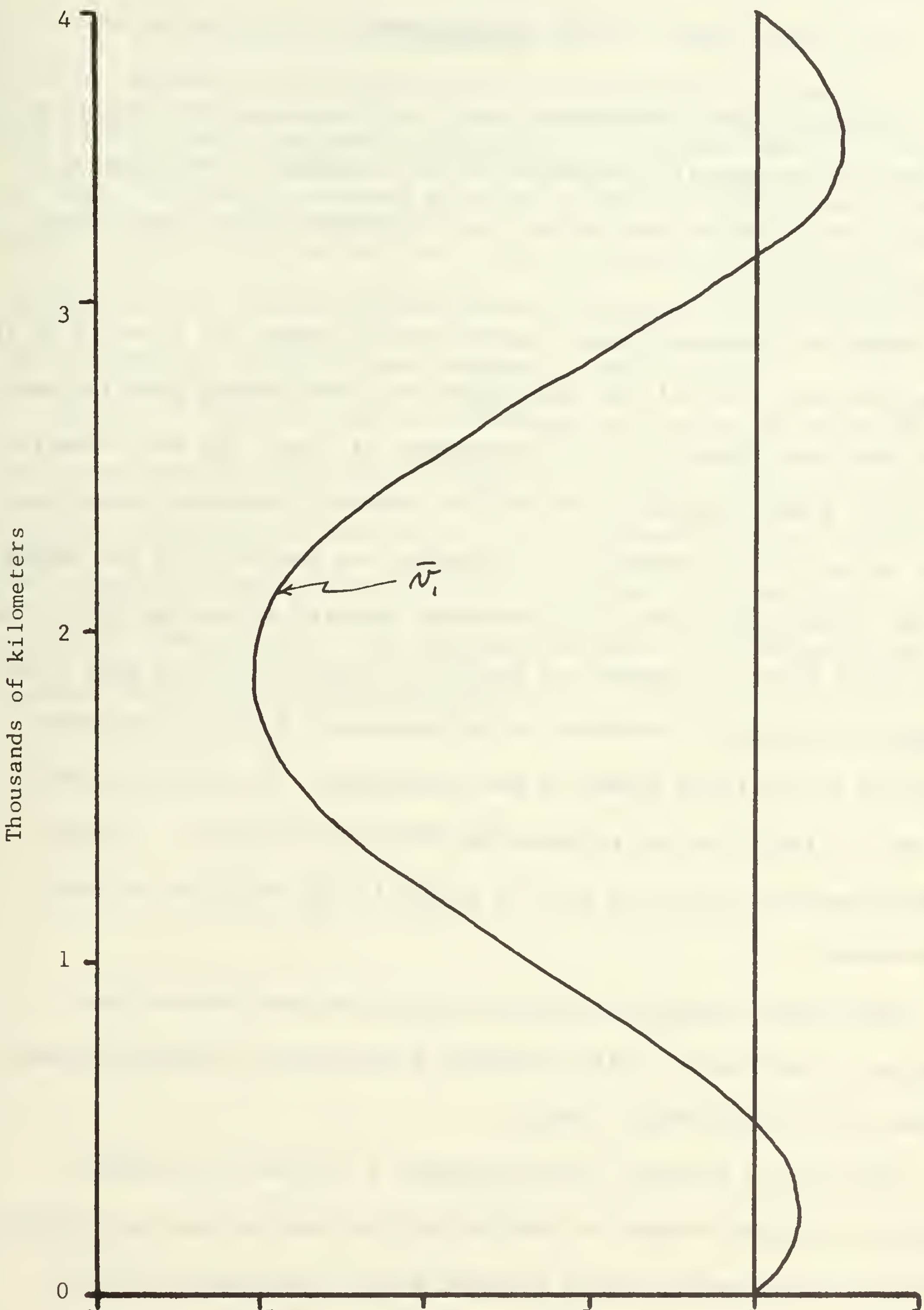

Fig. 14 - The Amplitude of the Mean Meridional Component of the Wind ($\bar{v}_1$) for day 200.

VI. CONCLUSIONS

A two-level quasi-geostrophic model was formulated for simplified studies of the general circulation of the atmosphere. The model was further simplified by restricting the disturbance to one wave in the zonal direction.

Numerical integration was computationally stable for a period of at least 300 days. In all the experiments the same heating function was used which was linear in y and independent of time. The main experiment with a wall separation of 8000 km produced fluctuating solutions with irregular time variations. Attention was focused on a sub period of the integration where the disturbance featured a rapid growth followed by a rapid decay. Apparently a double jet structure in the mean flow became barotropically unstable at the beginning of the period which resulted in the rapid growth of the disturbance. By the end of the period, a single jet had replaced the double jet structure. Energy transformations verify the roll of $[K' \cdot \overline{K}]$ in the evolution of this disturbance.

Experiment 2 featured a double heating rate and results were similar to experiment 1 with increased fluctuations and higher energy values of the disturbance energy.

Experiment 3 differed from experiment 1 in that the distance between walls was reduced to 4000 km and the heating rate was doubled. The disturbance energy became constant after approximately 120 days and remained so throughout the forecast period. This situation represents a wave of constant amplitude propagating through the atmosphere. The behavior resembles the flow observed in certain dishpan experiments which contained a central core [Hide, 1953; Fultz, et al, 1959]. Apparently the explanation of the difference in behavior between experiment 1 and experiment 3 is related to the fact that for W = 8000 km, at least two energy producing modes of disturbance energy can exist in y, whereas for W = 4000 km only one energy producing mode can exist. The presence of two energy producing modes apparently leads to fluctuations in time but the one modal case produces a steady wave.

Further studies utilizing this simple model could be performed such as longer period forecasting; changes in the form of heating; simulating dishpan experiments by setting $\beta = 0$ and concentrating the heating near the boundaries, and a change in the wave number k to name a few. Any or all of these studies could further enhance our understanding of the general circulation of the atmosphere.

APPENDIX A - COMPUTATION OF VERTICAL MOTION

The computation of vertical motion (ω_2) is necessary for the energy equation. To derive the computational equation for vertical motion, start with

$$\omega_2 = \frac{2}{\Delta p\sigma}\left[\frac{\partial \Psi_T}{\partial t} + u_m \frac{\partial \Psi_T}{\partial x} + v_m \frac{\partial \Psi_T}{\partial y} + \frac{\varkappa Q_2}{2}\right], \tag{A-1}$$

where

$$u_m = -\frac{1}{f_o}\frac{\partial \Psi_m}{\partial y} \tag{A-2}$$

$$v_m = \frac{1}{f_o}\frac{\partial \Psi_m}{\partial x} . \tag{A-3}$$

Substituting equations (A-2), (A-3), (2.15) and (2.16) into (A-1), collecting terms, and again neglecting terms with wave number 2k or higher results in

$$\omega_2 = \frac{2}{\Delta p\sigma}\left\{\cos kx\left[\frac{\partial C}{\partial t} - \frac{k}{f_o}\left(\frac{\partial E}{\partial y} D - \frac{\partial F}{\partial y} B\right)\right] + \right.$$

$$\left. \sin kx\left[\frac{\partial D}{\partial t} + \frac{k}{f_o}\left(\frac{\partial E}{\partial y} C - \frac{\partial F}{\partial y} A\right)\right] + \frac{\partial F}{\partial t} + \frac{\varkappa Q_2}{2}\right\} . \tag{A-4}$$

Both the disturbance and the average vertical motion are given by this equation, which is the equation used in the model for the computation of vertical motion.

APPENDIX B - COMPUTATION OF AVERAGE NORTH-SOUTH WIND

The computation of the average north-south wind $(\bar{v}_1)$ is necessary for the energy calculations. The computation for $\bar{v}_1$ can be derived from Fig. B-1 by the following

$$\frac{\partial \overline{\omega}^x}{\partial p} + \overline{\nabla \cdot \mathbb{V}}^x = 0 \qquad \text{(B-1)}$$

$$\frac{\partial \overline{\omega}^x}{\partial p} + \frac{\partial \bar{v}_1}{\partial y} = 0 \qquad \text{(B-2)}$$

$$\frac{\overline{\omega}_2^x}{\Delta p} + \frac{\partial \bar{v}_1}{\partial y} = 0 \qquad \text{(B-3)}$$

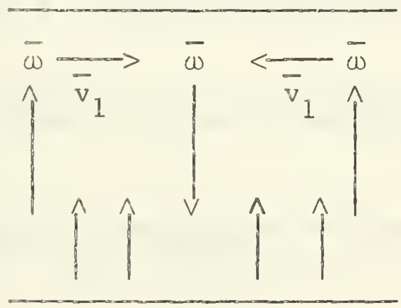

Fig. B-1

In finite difference form equation B-3 becomes

$$(\bar{v}_1)_1 = (\bar{v}_1)_i - \frac{\Delta y}{\Delta p}\left(\frac{(\bar{\omega}_2)_i + (\bar{\omega}_2)_{i+1}}{2}\right) \qquad \text{(B-4)}$$

with $v_1 = 0.0$.

APPENDIX C - ENERGY TRANSFORMATION EQUATIONS

The following definitions are utilized in the energy transformation equations of Phillips [1956]

Mean Potential Energy $\bar{P} = \frac{\mu^2}{W} \int \left(\frac{\bar{\Psi}_1 - \bar{\Psi}_3}{2} \right)^2 dy$ (C-1)

Disturbance Potential Energy $P' = \frac{\mu^2}{4W} \int \overline{(\Psi'_1 - \Psi'_3)^2}\, dy$ (C-2)

Mean Kinetic Energy $\bar{K} = \frac{1}{4W} \int (\bar{u}_1^2 + \bar{u}_3^2)\, dy$ (C-3)

Disturbance Kinetic Energy $K' = \frac{1}{2W} \int \overline{\left[\left(\frac{\partial \Psi'_1}{\partial x} \right)^2 + \left(\frac{\partial \Psi_1}{\partial y} \right)^2 + \left(\frac{\partial \Psi'_3}{\partial x} \right)^2 + \left(\frac{\partial \Psi'_3}{\partial y} \right)^2 \right]}\, dy$

(C-4)

Phillips [1956] derived the following disturbance energy transformation equations which provide an excellent means for examining the extent to which the model contains the physical processes known to be important in the atmosphere.

$$[\bar{P} \cdot P'] = - \frac{\mu^2}{4W} \int \overline{v_1 (\Psi'_1 - \Psi'_3)}\, \frac{\partial}{\partial y} (\bar{\Psi}_1 - \bar{\Psi}_3)\, dy \qquad \text{(C-5)}$$

$$[P' \cdot K'] = - \frac{f_o}{2 p_2 W} \int \overline{\omega'_2 (\Psi'_1 - \Psi'_3)}\, dy \qquad \text{(C-6)}$$

$$[K' \cdot \bar{K}] = - \frac{1}{2W} \int \left[\bar{u}_1 \frac{\partial}{\partial y} (\overline{u'_1 v'_1}) + \bar{u}_3 \frac{\partial}{\partial y} (\overline{u'_3 v'_3}) \right] dy \qquad \text{(C-7)}$$

$$[K' \cdot A_H] = \frac{A_H}{2W} \int \overline{\left[(\zeta_1')^2 + (\zeta_3')^2 \right]}\, dy \qquad \text{(C-8)}$$

$$[K' \cdot A_v] = \frac{A_v}{2W} \int \mathbb{V}'_3 \cdot \mathbb{V}'_3\, dy \qquad \text{(C-9)}$$

The symbolic notation of the form $[\bar{P}\cdot P']$ for example, signifies a transformation of energy from one form - the first in the bracket - to the second form. The example $[\bar{P}\cdot P']$ represents the transformation of mean potential energy into the disturbance potential energy.

Utilizing equations (2.9), (2.10), (2.15) and (2.16), the components of the disturbance energy become

$$P' = \frac{\mu^2}{2W}\int_0^W (C^2 + D^2)\, dy \tag{C-10}$$

and

$$K' = \frac{1}{2W}\int_0^W \left[k^2(A^2+B^2+C^2+D^2) + \left(\frac{\partial A}{\partial y}\right)^2 + \left(\frac{\partial B}{\partial y}\right)^2 + \left(\frac{\partial C}{\partial y}\right)^2 + \left(\frac{\partial D}{\partial y}\right)^2\right] dy \tag{C-11}$$

Similarly, equations (C-5) through (C-9) become

$$[\bar{P}\cdot P'] = -\frac{k\mu^2}{W}\int_0^W (BC - AD)\frac{\partial F}{\partial y}\, dy \tag{C-12}$$

$$[P'\cdot K'] = -\frac{1}{\Delta p W}\int_0^W [(WC)\, C + (WS)\, D]\, dy \tag{C-13}$$

$$[K'\cdot\bar{K}] = -\frac{k}{W}\int_0^W \left[\frac{\partial E}{\partial y}\left(B\frac{\partial^2 A}{\partial y^2} - A\frac{\partial^2 B}{\partial y^2} + D\frac{\partial^2 C}{\partial y^2} - C\frac{\partial^2 D}{\partial y^2}\right) + \right.$$

$$\left.\frac{\partial F}{\partial y}\left(B\frac{\partial^2 C}{\partial y^2} - C\frac{\partial^2 B}{\partial y^2} + D\frac{\partial^2 A}{\partial y^2} - A\frac{\partial^2 D}{\partial y^2}\right)\right] dy \tag{C-14}$$

$$[K'\cdot A_H] = \frac{A_H}{W}\int_0^W \left\{\left[\left(\frac{\partial^2}{\partial y^2} - k^2\right)A\right] + \left[\left(\frac{\partial^2}{\partial y^2} - k^2\right)B\right]^2 + \right.$$

$$\left.\left[\left(\frac{\partial^2}{\partial y^2} - k^2\right)C\right]^2 + \left[\left(\frac{\partial^2}{\partial y^2} - k^2\right)D\right]^2\right\} dy \tag{C-15}$$

$$[K' \cdot A_V] = \frac{1}{2} \frac{A_V}{W} \int_0^W \left\{ k^2 \left[(A-C)^2 + (B-D)^2 \right] + \left[\left(\frac{\partial C}{\partial y} - \frac{\partial A}{\partial y} \right)^2 + \left(\frac{\partial D}{\partial y} - \frac{\partial B}{\partial y} \right)^2 \right] \right\} dy \qquad \text{(C-16)}$$

LIST OF REFERENCES

Bryan, K., 1959: A numerical integration of certain features of the general circulation. Tellus 11, 163-174.

Fultz, D. et al, 1959: Studies of thermal convection in a rotating cylinder with some implications for large scale atmospheric motions. Meteorological Monographs, Boston, American Meteorological Society, 4, 21, 104 pp.

Hide, R., 1953: Some experiments on thermal convection in a rotating liquid. Quarterly Journal of the Royal Meteorological Society, 79, 161.

Kuo, H. L., 1949: Dynamic instability of a two-dimensional non-divergent flow in a barotropic atmosphere. Journal of Meteorology, Vol. 6, 105-122.

Kurihara, Yoshhio and J. L. Holloway, Jr., 1967: Numerical integration of a nine-level global primitive equation model formulated by the box method. Monthly Weather Review, Vol. 95, No. 8, 509-530.

Kasahara, A. and W. M. Washington, 1967: NCAR global general circulation model of the atmosphere. Monthly Weather Review, Vol. 95, No. 7, 389-402.

Lorenz, E. N., 1962: Simplified dynamic equations applied to the rotating-basin experiment. Journal of Atmospheric Sciences, 19, 39-51.

Lorenz, E. N., 1963: The mechanics of vacillation. Journal of Atmospheric Sciences, 20, 448-464.

Manabe, Syukuro, 1969: The atmospheric circulation and the hydrology of the earth's surface. Monthly Weather Review, Vol. 97, No. 11, 739-774.

Manabe, Syukuro and J. Smagorinsky, 1967: Simulated climatology of a general circulation model with a hydrologic cycle: II. Analysis of the tropical atmosphere. Monthly Weather Review, Vol. 95, No. 4, 155-169.

Matsuno, J., 1966: Numerical integrations of the primitive equations by a simulated backward difference method. Journal of Meteorological Society of Japan, 44, 76-84.

Mintz, Y., 1965: Very long-term global integration of the primitive equations of atmospheric motion. WMO Technical Note No. 66, "WMO-IUGG Symposium on Research and Development Aspects of Long Range Forecasting, Boulder, Colo., 1964," Geneva, 1965, 141-167.

Nitta, Takashi, 1967: Dynamical interaction between the lower stratosphere and the troposphere. Monthly Weather Review, Vol. 95, No. 6, 319-339.

Phillips, N. A., 1956: The general circulation of the atmosphere. A numerical experiment. Quarterly Journal of the Royal Meteorological Society, Vol. 82, No. 352, 123-164.

Richtmyer, R. D., 1957: Difference Methods for Initial Value Problems. Interscience Publishers, Inc., New York.

Riehl, H., T. C. Yeh and N. E. LaSeur, 1950: A study of variations of the general circulation. Journal of Meteorology, Vol. 7, 181-194.

Smagorinsky, J., 1963: General circulation experiments with the primitive equation, I. The basic experiment. Monthly Weather Review, Vol. 91, No. 3, 99-165.

Smagorinsky, J., S. Manabe and J. L. Holloway, Jr., 1965: Numerical results from a nine-level general circulation model of the atmosphere. Monthly Weather Review, Vol. 93, No. 12, 727-768.

Thompson, P. D., 1961: Numerical Weather Analysis and Prediction. The MacMillan Company, New York.

Young, J. A., 1966: On the relation between zonal heating asymmetries and large-scale atmospheric fluctuations in space and time. Doctoriate Thesis, Massachusetts Institute of Technology, Cambridge, Massachusetts.

INITIAL DISTRIBUTION LIST

		No. Copies
1.	Library Naval Postgraduate School Monterey, California 93940	2
2.	Defense Documentation Center Cameron Station Alexandria, Virginia 22314	20
3.	Naval Weather Service Command Washington Navy Yard Washington, D. C. 20390	1
4.	Officer in Charge Naval Weather Research Facility Naval Air Station, Building R-48 Norfolk, Virginia 23511	1
5.	Commanding Officer U. S. Fleet Weather Central COMNAVMARIANAS, Box 12 FPO San Francisco, California 96630	1
6.	Commanding Officer Fleet Weather Central Box 110 FPO San Francisco, California 96610	1
7.	Commanding Officer U. S. Fleet Weather Central Box 31 FPO New York, New York 09540	1
8.	Commanding Officer Fleet Numerical Weather Central Naval Postgraduate School Monterey, California 93940	1
9.	ARCRL - Research Library L. G. Hanscom Field Attn: Nancy Davis/Stop 29 Bedford, Massachusetts 01730	1
10.	Director, Naval Research Laboratory Attn: Tech. Services Info. Officer Washington, D. C. 20390	1

11. American Meteorological Society 1
45 Beacon Street
Boston, Massachusetts 02128

12. Department of Meteorology 3
Code 51
Naval Postgraduate School
Monterey, California 93940

13. Department of Oceanography 1
Code 58
Naval Postgraduate School
Monterey, California 93940

14. Office of Naval Research 1
Department of the Navy
Washington, D. C. 20360

15. Commander, Air Weather Service 2
Military Airlift Command
U. S. Air Force
Scott Air Force Base, Illinois 62226

16. Atmospheric Sciences Library 1
Environmental Science Services Administration
Silver Spring, Maryland 20910

17. Professor Victor Starr 1
Department of Meteorology
M. I. T.
Cambridge, Massachusetts 03139

18. Dr. J. Pedlosky 1
Department of Geophysical Sciences
University of Chicago
Chicago, Illinois 60637

19. Dr. Joanne Simpson 1
Experimental Meteorology Branch
Environmental Science Services Administration
Coral Gables, Florida 33124

20. Dr. V. Jurcec 1
United Nations Development Program
Box 982
Cairo, United Arab Republic

21. Dr. A. Huss 1
Department of Meteorology
Hebrew University
Jerusalem, Isreal

22. National Center for Atmospheric Research 1
Box 1470
Boulder, Colorado 80302

23. Dr. T. N. Krishnamurti 1
Department of Meteorology
Florida State University
Tallahassee, Florida 32306

24. Dr. Fred Shuman 1
Director
National Meteorological Center
Environmental Science Services Administration
Suitland, Maryland 20390

25. Dr. J. Smagorinsky 1
Director
Geophysical Fluid Dynamics Laboratory
Princeton University
Princeton, New Jersey 08540

26. Professor N. A. Phillips 1
54-1422
M. I. T.
Cambridge, Massachusetts 02139

27. Professor J. G. Charney 1
54-1424
M. I. T.
Cambridge, Massachusetts 02139

28. Dr. E. N. Lorenz 1
Department of Meteorology
M. I. T.
Cambridge, Massachusetts 02139

29. Professor K. Ooyama 1
Department of Meteorology
New York University
University Heights
New York, New York 10453

30. Dr. M. G. Wurtele 1
Department of Meteorology
UCLA
Los Angeles, California 90024

31. Dr. A. Arakawa 1
Department of Meteorology
UCLA
Los Angeles, California 90024

32. Captain Thomas Kent Schminke 1
2107 Randal Drive
Bellevue, Nebraska 68005

33. Dr. David Houghton 1
Department of Meteorology
University of Wisconsin
Madison, Wisconsin 53706

34. Dr. S. K. Kao 1
Department of Meteorology
University of Utah
Salt Lake City, Utah 84112

35. Professor J. Holmboe 1
Department of Meteorology
UCLA
Los Angeles, California 90024

36. Dr. J. Holton 1
Department of Atmospheric Sciences
University of Washington
Seattle, Washington 98105

37. Dr. P. Gilma 1
Department of Astro-Geophysics
University of Colorado
Boulder, Colorado 80302

38. Dr. P. Thompson 1
National Center for Atmospheric Research
Box 1470
Boulder, Colorado 80302

39. Dr. Peter Stone 1
Pierce Hall
Harvard University
Cambridge, Massachusetts 02138

40. Dr. John Young 1
Department of Meteorology
University of Wisconsin
Madison, Wisconsin 53706

41. Dr. George J. Haltiner 1
Department of Meteorology
Naval Postgraduate School
Monterey, California 93940

42. Dr. Jerry D. Mahlman 1
Department of Meteorology
Naval Postgraduate School
Monterey, California 93940

43. Dr. Russell Elsberry 1
Department of Meteorology
Naval Postgraduate School
Monterey, California 93940

44. Commanding Officer 1
Pacific Missile Range
Attn: Geophysics Division
Point Mugu, California 93041

45. Commander R. L. Newman 1
Fleet Weather Facility
Box 72
FPO New York, New York 09501

46. Dr. Roger Terry Williams 10
Department of Meteorology
Naval Postgraduate School
Monterey, California 93940

47. Lieutenant Commander Frank H. Taylor 5
U. S. Fleet Weather Central
Box 113
FPO San Francisco, California 96610

Security Classification

DOCUMENT CONTROL DATA - R & D

(Security classification of title, body of abstract and indexing annotation must be entered when the overall report is classified)

1. ORIGINATING ACTIVITY (Corporate author) Naval Postgraduate School Monterey, California 93940	2a. REPORT SECURITY CLASSIFICATION Unclassified 2b. GROUP

3. REPORT TITLE

General Circulation Experiments with a Two-Level Quasi-Geostrophic Model Including the Non-Linear Interaction Between a Single Wave in the Zonal Direction and the Mean Flow

4. DESCRIPTIVE NOTES (Type of report and inclusive dates)

Master's Thesis; April 1970

5. AUTHOR(S) (First name, middle initial, last name)

Frank H. Taylor

6. REPORT DATE	7a. TOTAL NO. OF PAGES	7b. NO. OF REFS
April 1970	50	20

8a. CONTRACT OR GRANT NO.	9a. ORIGINATOR'S REPORT NUMBER(S)
b. PROJECT NO.	
c.	9b. OTHER REPORT NO(S) (Any other numbers that may be assigned this report)
d.	

10. DISTRIBUTION STATEMENT

This document has been approved for public release and sale; its distribution is unlimited.

11. SUPPLEMENTARY NOTES	12. SPONSORING MILITARY ACTIVITY
	Naval Postgraduate School Monterey, California 93940

13. ABSTRACT

A long-period forecast is made utilizing a two-level quasi-geostrophic model. The model includes friction and heating which is a linear function of y. The model was further simplified by restricting the disturbance to one wave in the zonal direction. Experiments were performed with two distances between the walls. In the case of the longer separation, a solution with appreciable time fluctuations was obtained with the largest fluctuation being investigated in more detail. The smaller separation revealed a traveling wave of constant amplitude similar to that observed in certain dishpan experiments.

14 KEY WORDS	LINK A		LINK B		LINK C	
	ROLE	WT	ROLE	WT	ROLE	WT
Two-level model						
Quasi-geostrophic						
Heating and friction						
Energy transformation						
General circulation						

Thesis 118274
T212 Taylor
c.1
General circulation experiments with a two-level quasi-geostrophic model including the non-linear interaction between a single wave in the zonal direction and the mean flow.